2016

# A Study on High Efficiency Wing-vane Compressor - Part.1: A Simulation Analysis of Dynamic Model -

Raito Kawamura
*Mitsubishi Electric Corporation, Japan*, kawamura.raito@cj.mitsubishielectric.co.jp

Shin Sekiya
*Mitsubishi Electric Corporation, Japan*, sekiya.shin@eb.mitsubishielectric.co.jp

Tatsuya Sasaki
*Mitsubishi Electric Corporation, Japan*, sasaki.tatsuya@ea.mitsubishielectric.co.jp

Hideaki Maeyama
*Mitsubishi Electric Corporation, Japan*, maeyama.hideaki@dx.mitsubishielectric.co.jp

Shinichi Takahashi
*Mitsubishi Electric Corporation, Japan*, takahashi.shinichi@bk.mitsubishielectric.co.jp

***See next page for additional authors***

**Authors**
Raito Kawamura, Shin Sekiya, Tatsuya Sasaki, Hideaki Maeyama, Shinichi Takahashi, and Kanichiro Sugiura

# A Study on High Efficiency Wing-vane Compressor - Part 1: A Simulation Analysis of Dynamic Model -

Raito KAWAMURA[1]*, Shin SEKIYA[2], Tatsuya SASAKI[3], Hideaki MAEYAMA[4], Shinichi TAKAHASHI[5], Kanichiro SUGIURA[6]

[1, 2, 3] Mitsubishi Electric Corporation, Advanced Technology R&D Center,
8-1-1 Tsukaguchi-Honmachi, Amagasaki, Japan
Phone: +81-6-6497-7173, Fax: +81-6-6497-7285,
[1] Email: Kawamura.Raito@cj.MitsubishiElectric.co.jp
[2] Email: Sekiya.Shin@eb.MitsubishiElectric.co.jp
[3] Email: Sasaki.Tatsuya@ea.MitsubishiElectric.co.jp

[4] Mitsubishi Electric Corporation, Living Environment Systems Laboratory,
3-18-1 Oshika, Suruga-ku, Shizuoka, Japan
Phone: +81-54-287-3053, Fax: +81-54-287-3056,
Email: Maeyama.Hideaki@dx.MitsubishiElectric.co.jp

[5, 6] Mitsubishi Electric Corporation, Shizuoka Works,
3-18-1 Oshika, Suruga-ku, Shizuoka, Japan
Phone: +81-54-287-3112, Fax: +81-54-287-3127,
[5] Email: Takahashi.Shinichi@bk.MitsubishiElectric.co.jp
[6] Email: Sugiura.Kanichiro@ay.MitsubishiElectric.co.jp

## ABSTRACT

Low global warming potential refrigerants such as HFO (hydro fluoro olefin) -1234yf are attractive as alternative working fluids in air-conditioning and cooling systems to address global warming. However, larger compressor sizes were required due to the lower fluid density compared with conventional refrigerants such as R410A. Thus, a new wing-vane compressor which has no contact between the vane and cylinder has been developed to prevent on increase in size without performance degradation. The wing-vane type has higher compression efficiency compared to the conventional sliding-vane type as it has no friction loss on the vane tip and it can significantly reduce the mechanical loss for the conventional sliding-vane type. Since the structure of the wing-vane type is different from the conventional vane type, the load characteristics on the rotor and vanes are completely different from the conventional vane type. Therefore, the compression characteristics and the load characteristics were investigated by creating a dynamic model of the wing-vane type. The results are as follows: (1) Characteristics of torque and load are equivalent to those of the conventional vane type. (2) Lubrication of the newly added partial arc guide bearings is important to ensure reliability.

## 1. INTRODUCTION

Low global warming potential refrigerants such as HFO-1234yf are attractive as alternative working fluids in air-conditioning and cooling systems to address global warming. However, larger compressor sizes were required due to the lower fluid density compared with conventional refrigerants such as R410A. Thus, a new wing-vane compressor which has no contact between the vane and cylinder has been developed to prevent an increase in size without performance degradation. In this paper, we introduce the basic structure and the operation principles of the wing-vane type, and describe the load and torque characteristics revealed by the simulation analysis of a dynamic model. In addition, the features and problems of the wing-vane type are described at the end.

## 2. BASIC STRUCTURE

Figure 2.1 shows the basic structure of wing-vane type. In order to compare it with the conventional sliding-vane type, the number of vanes in the wing-vane type was selected as two. Figure 2.1a is a longitudinal-section view and Figure 2.1b shows the disassembly view of the compression mechanism. The compression mechanism is accommodated under the shell, and it is composed of a frame, cylinder, cylinder-head, rotor, shaft, four bushes, and two wing-vanes. A wing-vane is composed of one vane and two vane-guides and the vane-guides are fitted into the groove in the frame and the cylinder-head. The outer periphery of the groove acts as a bearing to support the vane-guide, and its center coincides with the center of the cylinder. Therefore, the vane rotates around the center of the cylinder. Incidentally, the vane is inserted into the rotor to rotate with the rotor and the vane sides are supported with bushes which can change their position to face the center of cylinder.

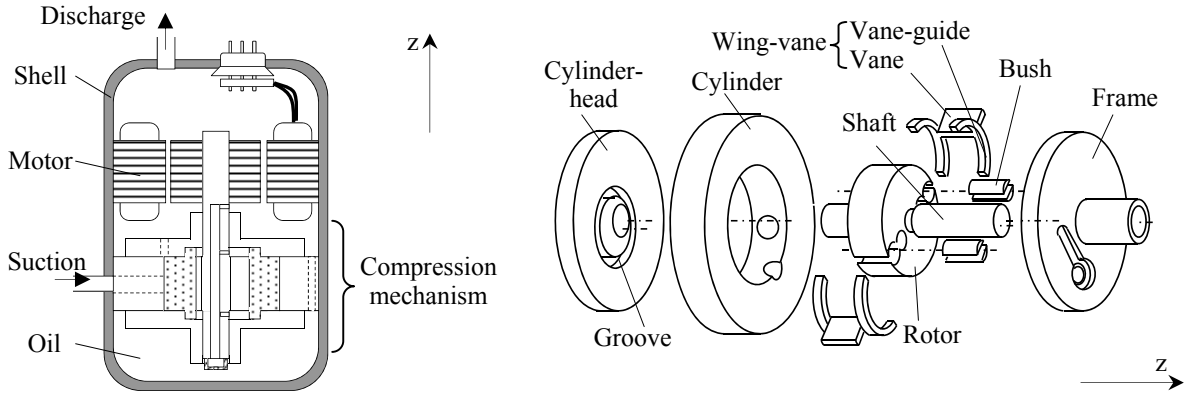


**(a)** Longitudinal section **(b)** Disassembly view of compression mechanism

**Figure 2.1:** Basic structure of wing-vane compressor

Figure 2.2 shows a horizontal cross-sectional view of the compression mechanism of the wing-vane type. It is compared the compression mechanisms of the rotary type, and the conventional sliding-vane type. Since in the rotary type, houses the vane in the cylinder, the cylinder outer diameter is larger than the other types of compressors. Since the sliding-vane type houses the vanes in the rotor, the cylinder outer diameter can be made smaller than the rotary type. However, since the tip of the vane rotates at high speed in contact with the inside of the cylinder, the performance is lower than the rotary type due to the increase of frictional losses. Further, since the vane doesn't rotate around the center of the cylinder, it is necessary to decrease the curvature of the vane tip rather than the cylinder inside. In the case of the wing-vane type, the vane is housed in the rotor and the tip of vane does not contact with the cylinder inside with the same curvature of vane tip. Therefore, the wing-vane type can achieve a high efficiency and small size using this structure.

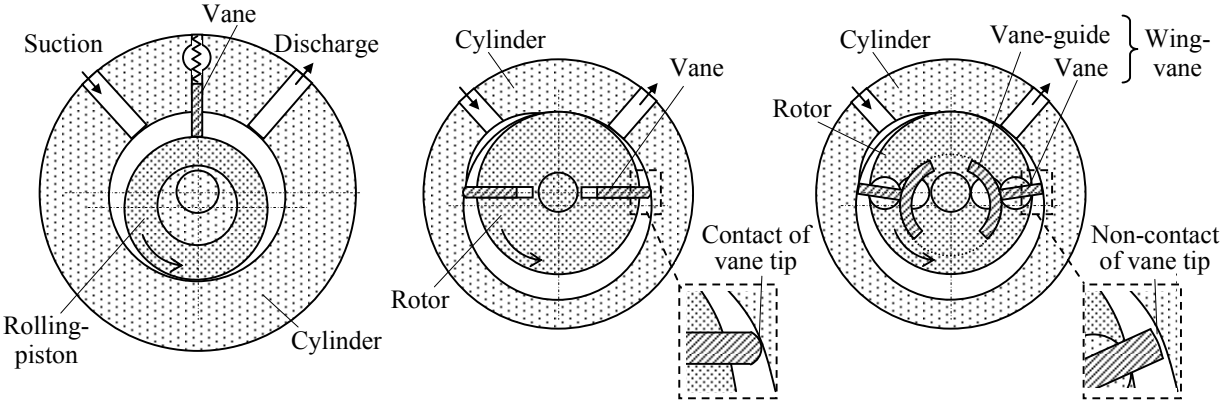


**(a)** Rotary **(b)** Sliding-vane **(c)** Wing-vane

**Figure 2.2:** Horizontal cross-sectional view of compression mechanisms

## 3. OPERATING PRINCIPLE

Figure 3.1 shows the compression process of the wing-vane type. Figure 3.1a shows the overall operation and Figure 3.1b shows the vane and the vane-guide operation. Because there are two vane, the compression process is completed at 180 degrees. The center chamber at 90 degrees is the timing when the suction process is completed, and then the compression process and the discharge process are started. As shown, the vane rotates around the center of the cylinder, so it is possible to keep the gap between the vane tip and the cylinder constant.

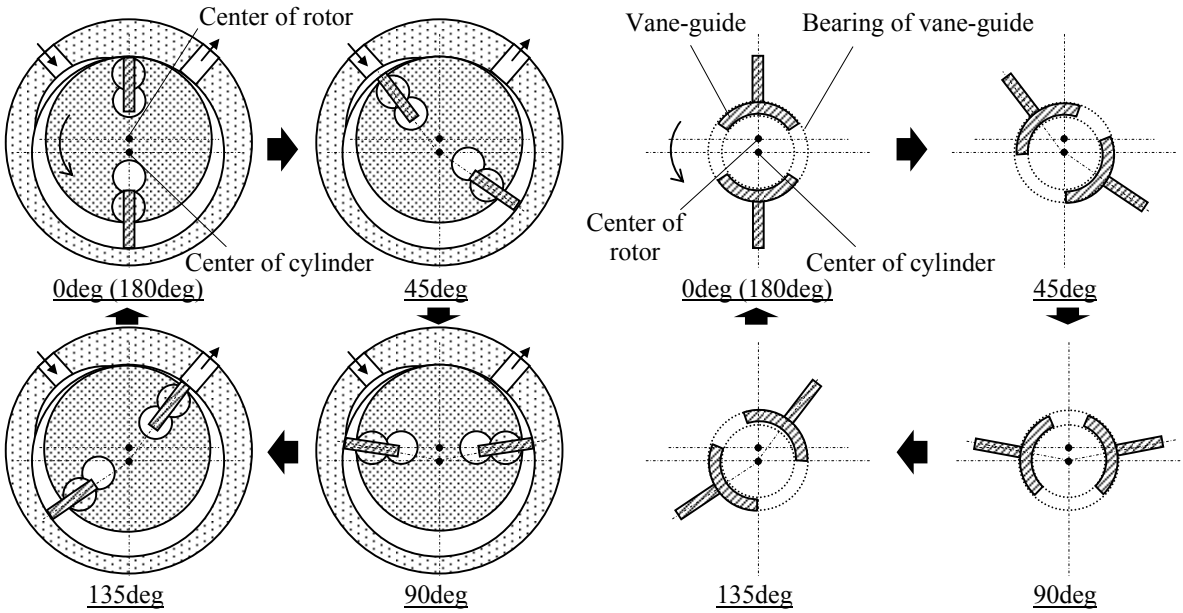


**(a)** Overall operation **(b)** Vane and vane-guide operation

**Figure 3.1:** Compression process of the wing-vane compressor

## 4. CHARACTERIZATION OF TORQUE AND ROTOR LOAD

### 4.1 Calculation of compression chamber volume change

Figure 4.1 shows the calculation model of the volume change in the compression chamber (with two vanes). This figure shows the symbols below: a: cylinder radius, b: rotor outside radius, e: cylinder eccentricity (= a-b), $r_s$: distance between center of rotor and the bush(ON), L (θ): distance between M and Q, $L_1$ (θ): distance between $O_c$ and N, $L_2$ (θ): distance between $O_c$ and M, O: center of rotor, $O_c$ : center of cylinder, P: proximity point, Q: tip of vane, M: intersection of line $O_cQ$ and outside of rotor, N: intersection of line $O_cQ$ and center line of bush, θ: ∠PON rotor rotation angle (P is set to 0 [deg]), φ:∠$PO_cM$, and ψ: ∠POM. For simplicity, the thickness of the vane is not taken into account in the drawing. The area A (θ) of the space enclosed between the 1st vane and point P can be obtained by the following equation (4.1),

$$A(\theta) = A_1 - A_2 - A_3 \tag{4.1}$$

Here, $A_1$: area of sector $PO_cQ$, $A_2$: area of sector POM, and $A_3$: area of $\Delta OO_cM$. Each of the areas is given by equation (4.2),

$$A_1 = \frac{a^2\phi}{2},\ A_2 = \frac{b^2\varphi}{2},\ A_3 = \frac{be\sin(\varphi)}{2} \tag{4.2}$$

Therefore, A (θ) is given by equation (4.1) and equation (4.2)

$$A(\theta) = \frac{a^2\phi}{2} - \frac{b^2\varphi}{2} - \frac{be\sin(\varphi)}{2} \tag{4.3}$$

Then, we find the angle φ and ψ. First, from the cosine theorem of $\Delta OO_cN$,

$$L_1(\theta) = \sqrt{r_s^2 + e^2 + 2r_s e\cos(\theta)} \quad (4.4)$$

$$r_s^2 = L_1(\theta)^2 + e^2 - 2L_1(\theta)e\cos(\phi) \quad (4.5)$$

From equations (4.4) and equation (4.5), φ is as follows,

$$\phi = \cos^{-1}\left(\frac{L_1(\theta)^2 + e^2 - r_s^2}{2L_1(\theta)e}\right) \ (0 < \theta < \pi) \quad (4.6)$$

$$\phi = 2\pi - \cos^{-1}\left(\frac{L_1(\theta)^2 + e^2 - r_s^2}{2L_1(\theta)e}\right) \ (\pi < \theta < 2\pi) \quad (4.7)$$

On the other hand, from the cosine theorem of $\Delta OO_cM$,

$$L_2(\theta) = e\cos(\phi) + \sqrt{b^2 - e^2\cos(\phi)^2} \quad (4.8)$$

$$L_2(\theta) = \sqrt{b^2 + e^2 + 2be\cos(\varphi)} \quad (4.9)$$

From equations (4.8) and equation (4.9), ψ is as follows;

$$\varphi = \cos^{-1}\left(\frac{L_2(\theta)^2 - b^2 - e^2}{2be}\right) \quad (0 < \theta < \pi) \quad (4.10)$$

$$\varphi = 2\pi - \cos^{-1}\left(\frac{L_2(\theta)^2 - b^2 - e^2}{2be}\right) \quad (\pi < \theta < 2\pi) \quad (4.11)$$

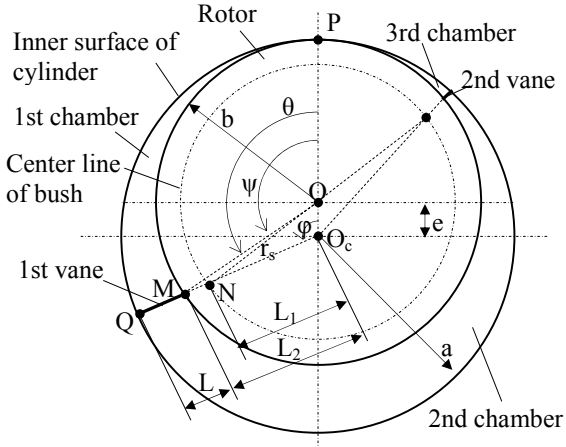


**Figure 4.1:** Calculation model of volume change in compression chamber

The areas of the 1st, 2nd, and 3rd chambers are $S_1$, $S_2$, and $S_3$, respectively and $S_1$, $S_2$, and $S_3$ are given by the following equation (4.12),

$$S_1 = A(\theta),\ S_2 = A(\theta + \pi) - A(\theta),\ S_3 = \pi(a^2 - b^2) - A(\theta + \pi) \quad (4.12)$$

The maximum compression chamber area $S_{max}$ is given by $\theta = \pi / 2$ in $S_2$ as follows,

$$S_{\max} = A(3\pi/2) - A(\pi/2) \quad (4.13)$$

Here, if the cylinder height is h, the suction volume $V_{st}$ is given by the following equation (4.14),

$$V_{st} = S_{\max} h \quad (4.14)$$

When considering the vane thickness $t_v$, the suction volume $V_{st}$* is given by the following equation (4.15),

$$V_{st}^{\ *} = [S_{\max} - \frac{t_v}{2}\{L(\frac{3\pi}{2}) + L(\frac{\pi}{2})\}]h \quad (4.15)$$

From Figure 4.1, L(θ) is given by the following equation (4.16),

$$L(\theta) = a - L_2(\theta) \quad (4.16)$$

It should be noted that in internal compression interval $\theta = \pi / 2 \sim \pi$, the internal volume ratio ε is given by the following equation (4.17),

$$\varepsilon = \frac{S_{\max}}{S_2(\pi) - S_{\max}} \quad (4.17)$$

## 4.2 Calculation of torque and load

Next, we will calculate the applied torque of vane $T_r$ and the applied load of rotor $F_r$. In Figure 4.2, $P_i(\theta)$ is the pressure applied on i-th chamber and $F_{pi}$ is the load applied on the i-th vane by the pressure difference, and $F_{si}$ is the applied load of the bush. $F_{p1}$ and $F_{p2}$ are as follows,

$$F_{p1} = L(\theta)h\{P_2(\theta) - P_1(\theta)\} \quad (4.18)$$

$$F_{p2} = L(\theta + \pi)h\{P_3(\theta) - P_2(\theta)\} \quad (4.19)$$

The applied torque of vane $T_r$ is as follows,

$$T_r = F_{p1}\{a - \frac{L(\theta)}{2} - e\cos(\phi)\} + F_{p2}\{a - \frac{L(\theta + \pi)}{2} - e\cos(\phi + \pi)\} \quad (4.20)$$

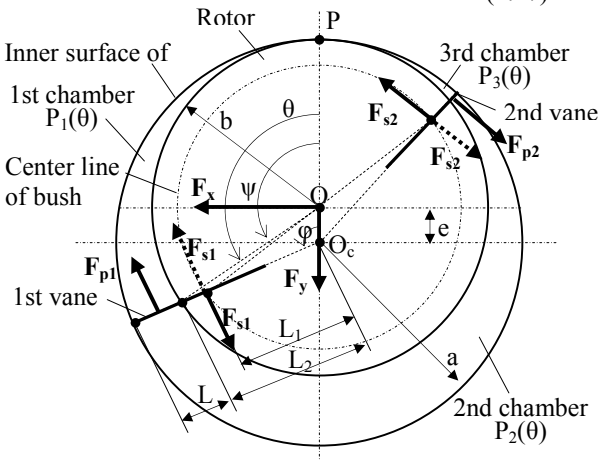


**Figure 4.2:** Calculation model of torque characteristics and the rotor load characteristics

$P_1(\theta)$, $P_2(\theta)$ and $P_3(\theta)$ have the following relationship,

$$P_2(\theta) = P_1\{\theta + \pi\}\ ,\ P_3(\theta) = P_1\{\theta + 2\pi\} \tag{4.21}$$

Next, we calculate the gas load applied on rotor $F_r$. Here $F_r$ is divided into the gas load applied on rotor $F_e$ and the gas load applied on bush $F_s$, where $F_s$ is generated by the vane load.

In Figure 4.2, $F_{exi}$, $F_{eyi}$ are the x-direction and y-direction components of the load applied on the rotor in each i-th chamber, $F_{exi}$ and $F_{eyi}$ are given by the following equations (4.22),

$$F_{ex1} = -bhP_1(\theta)\{1-\cos(\varphi)\}\ ,\ F_{ey1} = bhP_1(\theta)\sin(\varphi)\ ,\ F_{ex2} = -2bhP_2(\theta)\cos(\varphi)\ , \tag{4.22}$$

$$F_{ey2} = -2bhP_2(\theta)\sin(\varphi)\ ,\ F_{ex3} = bhP_3(\theta)\{1+\cos(\varphi)\}\ ,\ F_{ey3} = bhP_3(\theta)\sin(\varphi)$$

Here $F_{ex}$, $F_{ey}$ are the x-direction and y-direction components of $F_e$ and $F_{ex}$, and $F_{ey}$ is given by the following equations (4.23),

$$F_{ex} = F_{ex1} + F_{ex2} + F_{ex3}\ ,\quad F_{ey} = F_{ey1} + F_{ey2} + F_{ey3} \tag{4.23}$$

Next, we calculate the gas load applied on the rotor (bush) through the vanes $F_{s1}$ and $F_{s2}$. From the balance of the moment around the center of the cylinder, the following equations (4.24) are obtained,

$$F_{s1} = F_{p1}\frac{\{a-\frac{L(\theta)}{2}\}}{L_1(\theta)}\ ,\ F_{s2} = F_{p2}\frac{\{a-\frac{L(\theta+\pi)}{2}\}}{L_1(\theta+\pi)} \tag{4.24}$$

Here, $F_{s1}$ and $F_{s2}$ are applied on the rotor and bush. The x-direction and y -direction components of this load are $F_{sxi}$ and $F_{syi}$ respectively, and $F_{sxi}$ and $F_{syi}$ are given by following equations (4.25) - (4.28),

$$F_{sx1} = -\frac{L(\theta)}{L_1(\theta)}\{a-\frac{L(\theta)}{2}\}h\{P_2(\theta)-P_1(\theta)\}\cos(\phi) \tag{4.25}$$

$$F_{sy1} = -\frac{L(\theta)}{L_1(\theta)}\{a-\frac{L(\theta)}{2}\}h\{P_2(\theta)-P_1(\theta)\}\sin(\phi) \tag{4.26}$$

$$F_{sx2} = -\frac{L(\theta+\pi)}{L_1(\theta+\pi)}\{a-\frac{L(\theta+\pi)}{2}\}h\{P_3(\theta)-P_2(\theta)\}\cos(\phi+\pi) \tag{4.27}$$

$$F_{sy2} = -\frac{L(\theta+\pi)}{L_1(\theta+\pi)}\{a-\frac{L(\theta+\pi)}{2}\}h\{P_2(\theta)-P_1(\theta)\}\sin(\phi+\pi) \tag{4.28}$$

The x-direction and y -direction components of $F_s$ are $F_{sx}$ and $F_{sy}$, respectively, and $F_{sx}$ and $F_{sy}$ are given by the following equations (4.29),

$$F_{sx} = F_{sx1} + F_{sx2}\ ,\qquad F_{sy} = F_{sy1} + F_{sy2} \tag{4.29}$$

Here, $F_r$ is the applied load of the rotor, and $F_{rx}$ and $F_{ry}$ are the x-direction and y-direction components of $F_r$. So $F_{rx}$, $F_{ry}$ and $F_r$ are given by the following equations (4.30),

$$F_{rx} = F_{ex} + F_{sx}\ ,\qquad F_{ry} = F_{ey} + F_{sy}\ 、\qquad F_r = \sqrt{{F_{ey}}^2 + {F_{sy}}^2} \tag{4.30}$$

### 4.3 Characteristics comparison

Next, we compare the characteristics of the torque and the rotor load with the conventional sliding-vane type. For the comparison, it is assumed that the suction volume and cylinder inside diameter and the rotor outside diameter are the same. The basic dimensions are below: suction volume: $V_{st}$ = 28.5 [cc / rev], cylinder radius: a = 30 [mm], rotor outside radius: b = 25.5 [mm] and the vane thickness is ignored. The maximum chamber area of the wing-vane type is $S_{max}$, this is slightly larger than that of the sliding-vane type $S_{max}$*, $S_{max}$ / $S_{max}$* = 1.017. The compression chamber volume has almost identical characteristics, and is not shown. Accordingly, the characteristics of the torque and the rotor load have almost identical characteristics as shown in Figure 4.3 and Figure 4.4. These figures are the characteristics under specific operating conditions (evaporation temperature 52℃, condensation temperature 5℃).

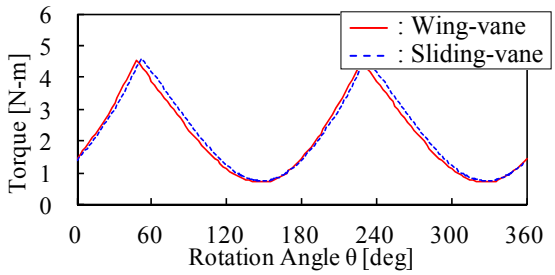


**Figure 4.3:** Characteristics of torque with respect to rotational phase

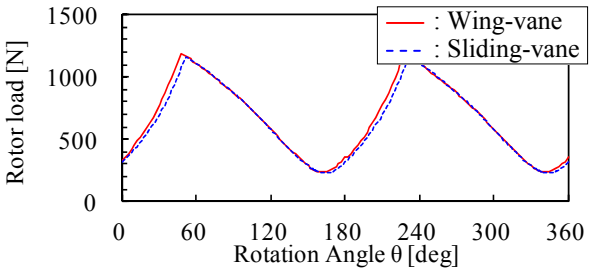


**Figure 4.4:** Characteristics of rotor load with respect to rotational phase

## 5. CHARACTERIZATION OF VANE LOAD

### 5.1 Constraints of arc angle of vane-guide

We now calculate the applied load of the vane-guide. The applied load of the vane is shown in Figure 5.1a, and the applied load of the vane-guide is shown in Figure 5.1b. In order to determine the load applied on only the 1st vane, the subscript is omitted. In Figure 5.1b, the arc of the vane-guide is asymmetric with respect to the vane, $\alpha_1$ is the arc angle from the center line of the vane measured in the rotational direction, and $\alpha_2$ is the arc angle from the center line of the vane measured in the counter-rotational direction.

Here, as described in Section 2, the circular arc angle $\alpha_1$ and $\alpha_2$ is limited, so this should be invastigated first. As shown in Figure 3.1b, the two vane-guides are closest to each other when θ is 90 degrees. In this phase, the angle between the 1st vane and the 2nd vane β is given by following equation (5.1),

$$\beta = 2\pi - \{\phi(\frac{3\pi}{2}) - \phi(\frac{\pi}{2})\} \tag{5.1}$$

On the other hand, since the portion of arc angle $\alpha_1$ and the portion of arc angle $\alpha_2$ are in the angular range of β, it is necessary that following relation (5.2) is established for non-contact,

$$\alpha_1 + \alpha_2 < \beta \tag{5.2}$$

From equations (5.1) and (5.2), the arc angle of a vane-guide has the following constraints (5.3),

$$\alpha_1 + \alpha_2 < 2\tan^{-1}(\frac{r_s}{e}) \tag{5.3}$$

### 5.2 Calculation of bearing load of vane-guide

In Figure 5.1, $F_b$ is the radial-direction load applied on the vane from the pressure difference between the back and the tip, $F_{cv}$ is the centrifugal force applied on the vane, $F_{ca}$ is the centrifugal force applied on the vane-guide, M is the longitudinal-direction of the vane, N is the orthogonal-direction of the vane, m is the central-direction of the vane-guide, n is the direction perpendicular to m, and $F_m$ and $F_n$ are the n-direction and m-direction loads applied on the bearing of the vane-guide. When ζ is the angle of m-direction and M-direction, $F_m$ and $F_n$ are as follows,

$$F_m = F_{ca} + \frac{F_b + F_{cv}}{2}\cos(\zeta) + \frac{F_s - F_p}{2}\sin(\zeta),\ F_n = -\frac{F_b + F_{cv}}{2}\sin(\zeta) + \frac{F_s - F_p}{2}\cos(\zeta) \tag{5.4}$$

Here, ζ is given by the following equation (5.5),

$$\zeta = \frac{\alpha_1 - \alpha_2}{2} \tag{5.5}$$

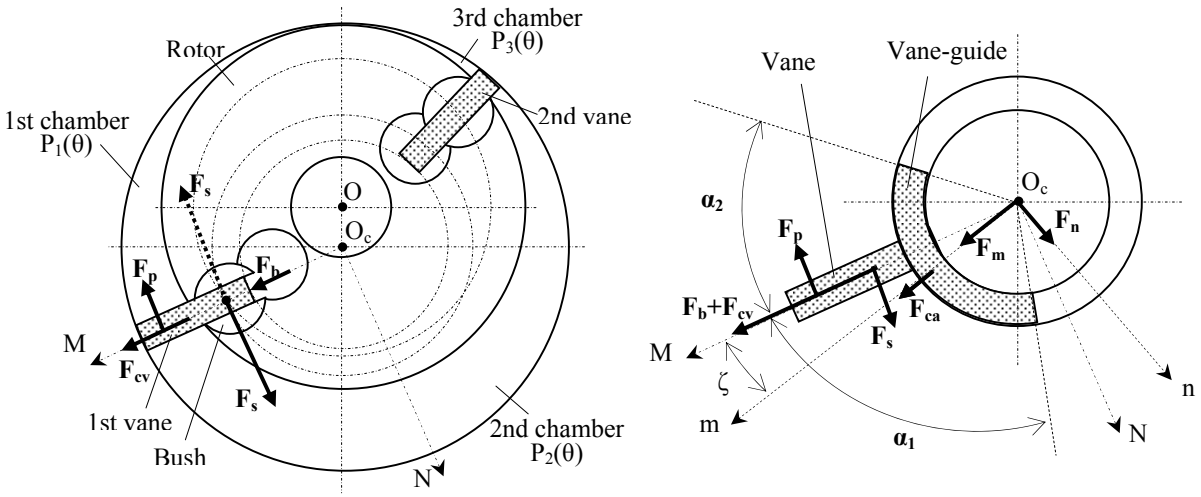


**(a)** Load applied on vane and bush **(b)** Load applied on vane-guide

**Figure 5.1:** Calculation model of vane-guide characteristics

The bearing of the vane-guide is a partial bearing which is different from an ordinary bearing. Therefore, the calculation method corresponding to a partial bearing is needed to calculate the characteristics of the vane-guide. The results of the calculation of partial bearing characteristics using a new calculation method are reported in Part 2

In the case of a partial bearing, when the ratio of $F_n$ for $F_m$ becomes larger, it can't be supported by the bearing surfaces of the vane-guide. In this situation, there is a risk that the wing-vane will be unstable. In this paper, a simple means of calculating the limit angle where the wing-vane is unstable is described. In Figure 5.2, $F_1$ and $F_2$ are the loads applied on the circumferential ends of the vane-guide. The vane-guide is assumed to be supported at two points. From the balance of forces, $F_1$ and $F_2$ are represented by the following equation (5.6),

$$F_1 = \frac{F_m \sin(\frac{\alpha_1+\alpha_2}{2}) + F_n \cos(\frac{\alpha_1+\alpha_2}{2})}{\sin(\alpha_1+\alpha_2)},\ F_2 = \frac{F_m \sin(\frac{\alpha_1+\alpha_2}{2}) - F_n \cos(\frac{\alpha_1+\alpha_2}{2})}{\sin(\alpha_1+\alpha_2)} \tag{5.6}$$

It is necessary for $F_2 > 0$ to prevent stable operation. Therefore, if following relation (5.7) is satisfied, the vane will be stable.

$$\frac{F_n}{F_m} < \tan(\frac{\alpha_1+\alpha_2}{2}) \tag{5.7}$$

Figure 5.3 shows a calculation example of $F_1$ and $F_2$. If both loads are greater than 0, the vane-guide can be stable and maintain reliability.

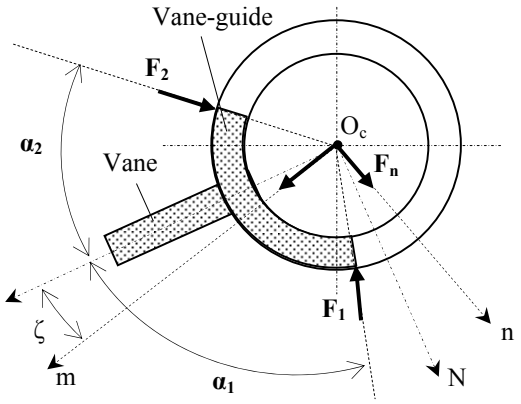


**Figure 5.2:** Calculation model of the stability of the vane-guide

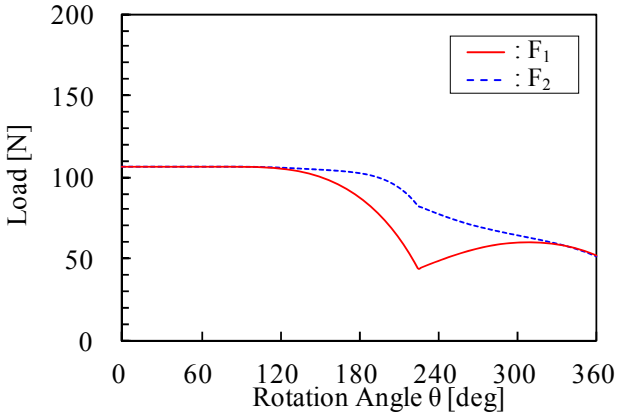


**Figure 5.3:** Characteristics of the stability of the vane-guide with respect to rotational phase

## 6. FEATURES AND PROBLEMS ON STRUCTURE

Next, we compare several features of the conventional sliding-vane type and the wing-vane type. We describe the comparison of the noteworthy matters as follows.

### 6.1 Compression Process, Torque, Rotor Load Characteristics

As indicated in Section 4.2, the characteristics of the chamber volume, torque, and rotor load are almost the same as the sliding-vane type. However, as will be described later, since the eccentricity must be smaller than the sliding-vane type, the rotor load tends to slightly increase over that of the sliding-vane type.

### 6.2 The size of the compression mechanism

Basically, since the center-direction of the vane tip curvature and the longitudinal-direction of the vane are constant, the operation of the wing-vane type is similar to that of the sliding-vane type. Therefore, it is necessary to increase the eccentricity which is smaller than that of the sliding-vane type which has longer vanes by deflecting the vane to the center of rotor (vane of general sliding-vane type is deflected). For this reason, the wing-vane type is slightly larger in the radial-direction than the sliding-vane type.

### 6.3 Performance

In the wing-vane type, the friction loss of the vane tip does not occur. However, a bearing loss in the vane-guide and a leakage loss in the vane tip clearance are now generated. If the sum of these losses is equal to the sum of the bearing loss inside the rolling-piston and the friction loss of the vane tip in the rotary type, the efficiency is expected to be the same as the rotary type.

### 6.4 Reliability

Since the vane-guide bearing and the bush are new frictional parts, it is necessary to ensure their reliability. In particular, as described above, since the vane-guide has a partial bearing, the stability of wing-vane operation is important. Therefore, it is necessary to understand the characteristics of the vane-guide bearing. The bush is used in the conventional swing compressor, but it was never used incorporated in the rotating body. Therefore, it is necessary to consider the frictional properties of the bush.

## 7. CONCLUSIONS

In this paper, a wing-vane compressor, which can achieve both high efficiency and downsizing, has been proposed and the characteristics of torque, rotor load and vane load were calculated. The characteristics of the wing-vane type is as follows.

・The striking feature of the wing-vane type is that there is no friction loss at the vane tip . Therefore, it eliminates the largest disadvantage of the sliding-vane type.
・ However, a leakage loss in the vane tip clearance and a bearing loss in the vane-guide are now generated. If the sum of these losses is equal to the sum of the bearing losses of the rolling-piston and the friction loss in the vane tip of the rotary type, the efficiency is expected to be the same as the rotary type.
・The characteristics of the compression process, torque, and rotor load, are almost the same as the sliding-vane type. However, since it is difficult to handle a large eccentricity, the applied load of the rotor is larger than the sliding-vane type.
・Lubrication of the newly added vane-guide and bush is important to ensure reliability.